Postural Arm Control Following Cervical Spinal Cord Injury

Eric J. Perreault, *Member, IEEE*, Patrick E. Crago, *Member, IEEE*, and Robert F. Kirsch, *Member, IEEE*

***Abstract*—This study used estimates of dynamic endpoint stiffness to quantify postural arm stability following cervical spinal cord injury (SCI) and to investigate how this stability was affected by functional neuromuscular stimulation (FNS). Measurements were made in the horizontal plane passing through the glenohumeral joint on three SCI-impaired arms, which ranged in functional level from a weak C5 to a strong C6. Endpoint stiffness, which characterizes the relationship between externally imposed hand displacements and the resultant forces, was estimated during the application of planar, stochastic perturbations to each arm. These estimates were used in conjunction with voluntary endpoint force measurements to quantify stability and strength during voluntary contractions and during voluntary contractions in the presence of triceps FNS. The primary findings were: 1) the differences in the force generating capabilities of these arms were due primarily to differences in shoulder strength; 2) measurements of strength alone could not be used to predict arm stability; and 3) triceps FNS improved postural arm stability for all tested conditions. These results suggest strategies for improved control of FNS systems designed to restore arm function following cervical SCI and underscore the importance of examining the effects of FNS on both strength and stability.**

***Index Terms*—Endpoint stiffness, functional neuromuscular stimulation, posture stability, spinal cord injury.**

I. Introduction

THIS study examined postural arm stability in individuals with C5-C6 level spinal cord injuries (SCI) and investigated how this stability was modified by functional neuromuscular stimulation (FNS) of the paralyzed triceps muscle. Able-bodied individuals use a large number of shoulder and elbow muscles to position the hand throughout the available workspace and to stabilize it at desired fixed positions [1]. Individuals with cervical SCI can move their hand through a much smaller workspace, restricting their ability to perform normal activities of daily living [2]–[4]. Because the primary goal of any rehabilitative effort is to restore function, traditional measures of arm impairment have centered on functional outcomes [4]–[7]. Unfortunately, detailed functional assessments are time-consuming, qualitative, and often provide limited insight to the mechanisms limiting functional performance. Previous studies have reported increases in elbow extension moments produced by FNS and related these to enhanced functional abilities during triceps FNS [8]–[10]. However, it is unclear whether the functional gains were due primarily to strength alone, to enhanced stability due to cocontraction of the stimulated triceps and voluntary biceps, or to some combination of the two.

In this work, estimates of dynamic endpoint stiffness were used to quantify the mechanical properties of the arm and to investigate arm stability. Endpoint stiffness is defined as the relationship between externally applied displacements of the hand and the forces generated in response. It characterizes the mechanical interface humans use to interact with their environment and therefore is thought to be related closely to postural stability. Numerous studies have quantified endpoint stiffness properties in able-bodied individuals [11]–[16]. Recently developed techniques [17] have allowed us to examine postural arm stability in individuals with SCI. This robust and efficient approach represents a practical clinical tool that also may be useful for quantifying the mechanical consequences of other neuromotor deficits, predicting functional outcomes of rehabilitative efforts to reduce these deficits and providing quantitative information regarding how these outcomes can be improved. If so, it would provide a valuable complement to the more traditional measures of neuromotor impairment.

TABLE I
ARM IMPAIRMENT LEVEL. INDICATES THE SIDE OF THE TESTED ARM, THE ASIA IMPAIRMENT LEVEL, AND THE MOTOR PORTION OF THE INTERNATIONAL TETRAPLEGIA HAND CLASSIFICATION

Limb	Side	ASIA Level	Int. Level
$C5^-$	L	C5	0
$C5^+$	R	C5	1
C6	L	C6	2

II. Methods

A. Experimental

Two subjects (three arms) with complete cervical-level spinal cord injuries (SCIs) that impaired arm function were examined in this study. Both subjects gave informed consent to all procedures and were free to withdraw from the study at any time. The left arm of one subject and both arms of a second subject with a nonsymmetrical injury were examined. The tested arms were selected based upon their differences in impairment. None had voluntary elbow extension and all had voluntary elbow flexion, but the strength of the three arms in elbow flexion and shoulder function varied over a wide range. Table I summarizes the impairment level for the subjects' arms in terms of the American

Manuscript received February 22, 2001; revised December 14, 2001. This work was supported by the Department of Veteran Affairs Rehabilitation Research and Development Service, the National Institute of Health, and the Cleveland FES Institute.

E. J. Perreault is with the Department of Physiology, Northwestern University Medical School, Chicago, IL 60611 USA, the Biomedical Engineering Department, Case Western Reserve University, Cleveland, OH 44106 USA, and also with Louis Stokes VA Medical Center, Cleveland, OH 44106 USA (e-mail: eperreault@northwestern.edu).

P. E. Crago and R. F. Kirsch are with the Biomedical Engineering Department, Case Western Reserve University, Cleveland, OH 44106 USA and also with the Louis Stokes VA Medical Center, Cleveland, OH 44106 USA.

Publisher Item Identifier S 1534-4320(01)11407-5.

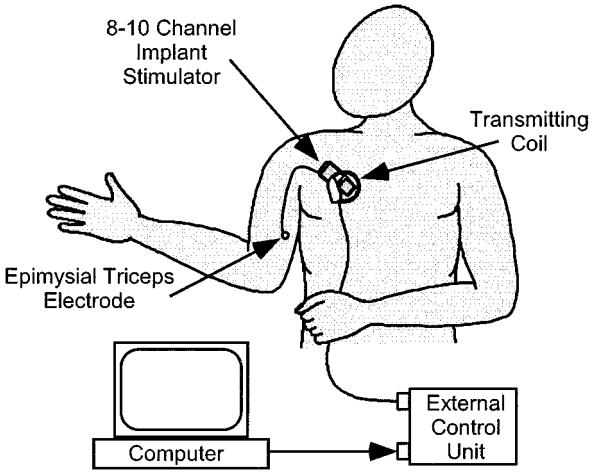

Fig. 1. Triceps FNS system. The portions of the implanted neuroprosthesis used for triceps stimulation are shown.

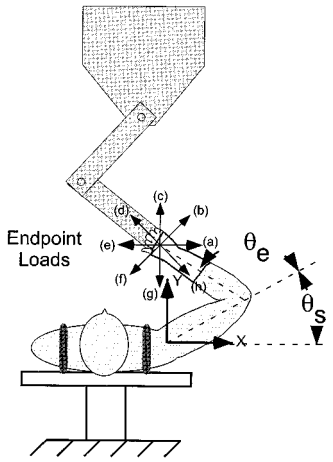

Fig. 2. Manipulator. A two-joint robotic manipulator was used to apply endpoint perturbations in these experiments. The manipulator was mounted on an adjustable structure, allowing its height to be customized for each subject. During each trial, subjects exerted a constant force on the manipulator in one of the eight directions shown.

Spinal Injury Association (ASIA) [18] classification and the International Tetraplegia Hand Classification [19], which are reasonable predictors of function for individuals with low cervical injuries [20]. The ASIA classification indicates the neurological level of injury and the international classification is used to plan surgical interventions according to which muscles below the elbow are available for transfer (higher numbers indicate more muscles available for transfer). The $-$ and $+$ superscripts associated with the C5 injury level provide additional detail on the impairment level, based upon the international classification and additional manual muscle tests of upper limb strength. In general, the $C5^-$ arm was weaker than the $C5^+$ arm, exhibiting a very weak brachioradialis (an elbow flexor) along with paralysis of the hand and wrist musculature. The C6 arm was stronger than both C5 arms.

Each arm had an implanted triceps neuroprosthesis to restore elbow extension [9], [10]. The triceps electrodes were part of a neuroprosthesis for restoring hand and elbow function following cervical SCI [21] and were not implanted for the purposes of this work. Fig. 1 illustrates the portions of the implant system relevant to this study. A single electrode receiving biphasic 20-mA current pulses from an implanted stimulator stimulated the triceps. Stimulation pulsewidth could be varied between 0–200 μsec and was set to the maximum functional value used by each subject, i.e., the largest pulsewidth below 200 μsec that did not result in spillover stimulation to a muscle other than the triceps. Prior to these experiments, the subjects' triceps muscles had been conditioned by months of daily electrically mediated exercise and were, therefore, resistant to fatigue [22]. An external unit controlled stimulator function and supplied the implanted stimulator with power via a coil placed on the chest surface.

Endpoint stiffness was estimated using perturbations applied by a two-joint robotic manipulator described previously [23]. Fig. 2 illustrates this device. For these experiments, the manipulator was configured as an endpoint position servo and was instrumented to measure endpoint force and position. During the experiments, the subject's trunk motion was constrained by firmly strapping him to his wheelchair. Chair movements were minimized by locking the wheels into place and securing the frame to an immovable wall via a rigid, adjustable length pole. Once the trunk and chair were secured, the subject's arm was attached to the endpoint of the manipulator via a custom-fitted fiberglass cast that was free to pivot in the horizontal plane about the attachment point.

Two identical sets of data were measured for each tested arm. These were collected on separate days, with at least one intervening day for rest. All measurements were made at a single location in the horizontal plane passing through the glenohumeral joint. In this plane, the subject's hand was positioned mediolaterally between the sternum and acromion at a distance approximately 0.45 m anterior to the acromion.

At the beginning of each experimental session, subjects were instructed to perform maximum voluntary contractions (MVCs) by exerting force against the manipulator in each of the eight directions shown in Fig. 2. Due to their motor impairments, subjects were able only to exert force in some of these directions. The MVC along each direction was defined as the maximum voluntary force that could be generated within $\pm 5^\circ$ of the target direction. The endpoint force generated by triceps stimulation was also measured by stimulating the triceps for 5 s and recording the maximum force sustained for at least 0.5 s. Three such measurements were made and averaged to provide a measure of triceps strength.

The second phase of each experimental session involved a series of endpoint stiffness measurements made: 1) at rest; 2) during voluntary muscle activation; 3) during stimulated triceps activation; and 4) during combined voluntary and stimulated muscle activation. The voluntary measurements were made while the subject exerted forces against the manipulator at 20% MVC along the directions shown in Fig. 2. Only directions where 20% MVC was greater than $2N$ were tested. Measurements with voluntary plus stimulated triceps activation were measured under two-endpoint loading conditions, with no net force at the hand-manipulator coupling and with an endpoint force of 20% MVC in the direction where the subject

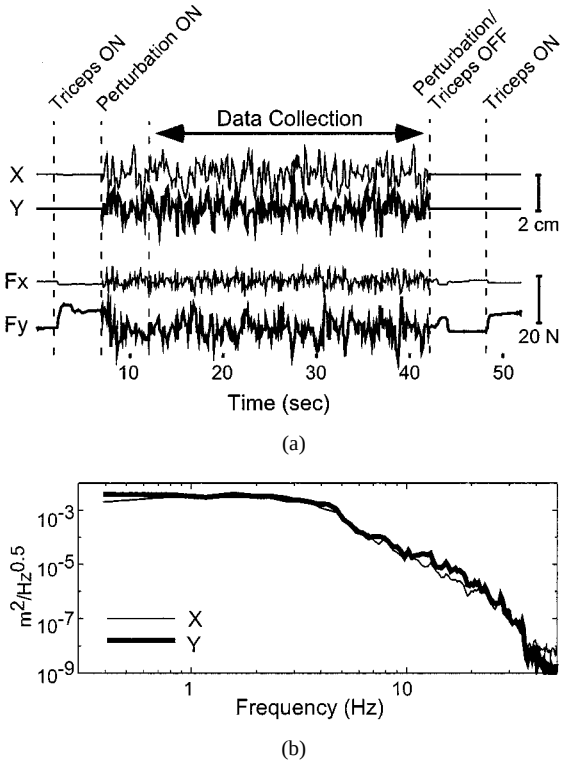

Fig. 3. Typical endpoint displacements and forces. (a) Typical displacements and forces during a single experimental trial. Dotted vertical lines indicate transition points in the experiment and are labeled above the figure. Only data between 12–42 s was used for subsequent analysis. (b) Power spectrum of the applied position perturbations.

was strongest. In both cases with triceps stimulation, the subject reached the target force using voluntary contractions to overcome the stimulated contraction. Fig. 3(a) shows typical experimental data and illustrates the sequence of events during each stiffness estimation trial. The top two traces represent the imposed endpoint displacements and the bottom two traces are the corresponding endpoint forces. The initial two seconds in each trial were used to quantify baseline levels. Triceps stimulation was then turned on so that the triceps contribution to endpoint force could be measured. At 7 s, the manipulator began to apply the stochastic displacements to the subject's hand and the subject was instructed to reach the target force within 5 s. The next 30 s of data was used to estimate the endpoint stiffness dynamics. At the end of this period, the stochastic displacements ceased, the triceps stimulation turned off and the subject stopped all voluntary contractions. After a period of 5 s, the triceps stimulation was again turned on to check for muscle fatigue between the beginning and end of the trial. The endpoint displacements had peak-to-peak amplitudes of approximately 2 cm, whereas the resulting endpoint force amplitudes varied from trial to trial depending upon the arm stiffness. Fig. 3(b) shows the spectra of the endpoint perturbations used in this study. The displacement frequency content was designed to be within the range of physiologically encountered perturbations [24] yet contain enough information for adequate identification of the endpoint dynamics. These perturbations were flat to 3 Hz, above which they decayed at a rate of 40 dB per decade.

B. Analytical

1) Nonparametric Endpoint Stiffness Estimation: Endpoint stiffness describes the dynamic relationship between displacements imposed at the hand and the forces generated by the arm in response to those displacements. Stiffness dynamics were estimated using a previously described nonparametric system identification algorithm [17], which assumes that, for small perturbations of hand position, endpoint stiffness dynamics can be approximated by a linear system [13], [14], [17], [25]. The linear dynamics equations describing the relationship between endpoint displacements and endpoint forces can be expressed succinctly in the frequency domain by (1), where f is frequency, $F_x(f)$ and $F_y(f)$ are the Fourier transforms of the endpoint forces, $X(f)$ and $Y(f)$ are the Fourier transforms of the endpoint displacements, and $H_{ij}(f)$ is the transfer function relating displacements in direction j to forces in direction i. The nonparametric algorithm estimates the optimal (least-squares) linear model for each of these single-input, single-output (SISO) subsystems

$$\begin{bmatrix} F_x(f) \\ F_y(f) \end{bmatrix} = \begin{bmatrix} H_{xx}(f) & H_{xy}(f) \\ H_{yx}(f) & H_{yy}(f) \end{bmatrix} \begin{bmatrix} X(f) \\ Y(f) \end{bmatrix}. \tag{1}$$

Coherence estimates [26] were used to examine the appropriateness of the linear approximation to the endpoint dynamics. Coherence ranges from zero to one, with regions of low coherence indicating insufficient input power, significant system nonlinearities, noise, or contributions from unmeasured inputs. Both *multiple* coherence (all inputs to a single output) and *partial* coherence (single inputs to single outputs) functions were computed.

2) Parameterization of Nonparametric Transfer Functions: Previous experimental studies have shown that, for small perturbations, each of the SISO systems contributing to the net endpoint stiffness dynamics can be approximated by system having inertial (I), viscous (B), and elastic (K) parameters [13], [14], as shown in (2). This parametric approximation was found to be adequate for our experimental data as well. The resulting parameterized system has the form given by (3). I_{end}, B_{end}, and K_{end} correspond to the endpoint inertia, viscosity, and static stiffness matrices, respectively. Inertial, viscous, and elastic parameters were fit to each of the nonparametric transfer functions using a Nelder-Mead multidimensional optimization algorithm (The Mathworks, Natick, MA 01760 USA). The squared error between the nonparametric and parametric transfer functions was weighted by the partial coherence to reduce the influence of poorly estimated portions of the transfer functions. Inertia was estimated only during the passive trials (where estimates are most accurate) and then fixed during the optimization for all remaining trials. Also, the combined force transducer and fiberglass cast inertia were measured separately and subtracted from the experimental inertia estimates. Hence, the reported results represent only arm inertia. The errors associated with the nonparametric system identification and the subsequent

parameter fits were evaluated using Monte Carlo simulations [16]

$$\begin{aligned} H_{ij}(s) &= I_{ij}s^2 + B_{ij}s + K_{ij}, \text{ where} \\ s &= 2\pi f\sqrt{-1} \\ [I_{\text{end}}][\ddot{x}] + [B_{\text{end}}][\dot{x}] + [K_{\text{end}}][x] &= [f_{\text{end}}] \text{ where} \\ [I_{\text{end}}] = \begin{bmatrix} I_{xx} & I_{xy} \\ I_{yx} & I_{yy} \end{bmatrix}, [B_{\text{end}}] &= \begin{bmatrix} B_{xx} & B_{xy} \\ B_{yx} & B_{yy} \end{bmatrix} \\ [K_{\text{end}}] = \begin{bmatrix} K_{xx} & K_{xy} \\ K_{yx} & K_{yy} \end{bmatrix}. \end{aligned} \quad (2), (3)$$

3) Graphical Representation of Parameter Fits: The inertial, viscous, and elastic properties of the arm are directionally dependent, meaning that the resistance that they provide to external perturbations of arm posture depends upon the orientation of the perturbation relative to the hand. This dependence on direction can be represented graphically by transforming the inertial, viscous, and elastic matrices into ellipses, as was first demonstrated by Mussa-Ivaldi [27]. Equation (4) shows this mapping for the endpoint elasticity matrix, K_{end}. The variables $F_y^K(t)$ and $F_x^K(t)$ represent the elastic components of the force response for unit displacements in endpoint position along all directions in the plane. The ellipse representing the directional properties of K_{end} is generated by plotting $F_y^K(t)$ against $F_x^K(t)$. A similar procedure is used to generate the viscosity and inertial ellipses. The major axis of each parameter ellipse denotes the direction along which the parameter is most significant and the minor axis denotes the direction along which the parameter is least significant

$$\begin{bmatrix} F_x^K(t) \\ F_y^K(t) \end{bmatrix} = K_{\text{end}} \cdot \begin{bmatrix} \cos(t) \\ \sin(t) \end{bmatrix} \text{ where } 0 < t < 2\pi. \quad (4)$$

4) Simulations of Endpoint Dynamics: A series of simulations was performed to characterize the two-dimensional (2-D) spatial response of the arm to force impulses applied in different directions. The inertial, viscous, and elastic parameters estimated for each experimental condition were combined, using the state-space representation shown in (5). The dynamic response to perturbations of endpoint position was investigated by simulating the endpoint trajectories resulting from a $1N$ force impulse applied at 16 equally spaced orientations in the measurement plane. These simulations provided a set of 2-D impulse response functions representing the endpoint position trajectory that would be evoked by these force impulses. Fig. 4 shows the results of one such simulation. The left portion of the figure shows the orientation of the force impulse applied to the hand and the right half shows the corresponding endpoint trajectory (arbitrary scale). For this particular perturbation, the endpoint oscillated approximately along the direction of the applied perturbation. The path length of the endpoint displacement trajectory was used as a quantitative measure of endpoint stability, with shorter path lengths corresponding to more stable arm postures

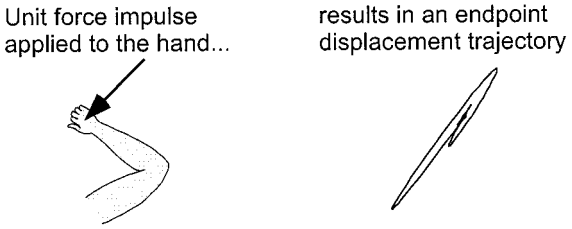

Fig. 4. Simulated transient responses. Illustrates the simulated endpoint trajectory in response to a unit impulse in endpoint force. The left portion shows the orientation of the force impulse and the right portion shows the corresponding endpoint trajectory (arbitrary scale). Arm parameters used during each such simulation were estimated from experimental data.

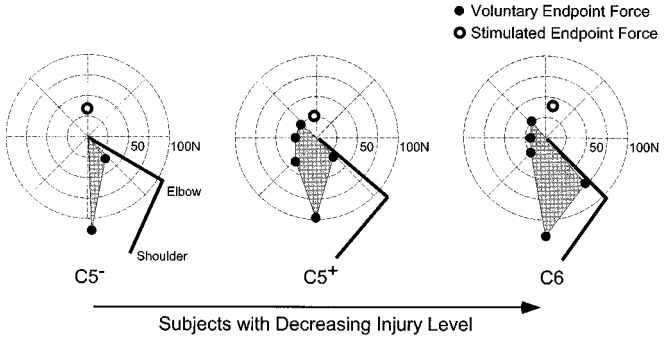

Fig. 5. Maximum voluntary endpoint forces. Shows the maximum forces generated by each of the tested arms along the measurement directions. The solid circles indicate the maximum voluntary forces and the open circles show the forces generated by triceps stimulation. The thick solid lines denote arm orientation. Note that all results are referenced to a right arm configuration.

$$\begin{aligned} \dot{x} &= Ax + Bu \\ y &= Cx + Du \quad \text{where} \\ A &= \begin{bmatrix} 0 & I \\ -I_{\text{end}}^{-1} \cdot K_{\text{end}} & -I_{\text{end}}^{-1} \cdot B_{\text{end}} \end{bmatrix} \\ B &= \begin{bmatrix} 0 \\ I_{\text{end}}^{-1} \end{bmatrix} \quad C = \begin{bmatrix} I \\ 0 \end{bmatrix} \quad D = 0. \end{aligned} \quad (5)$$

III. Results

A. Endpoint Force

Fig. 5 shows the MVCs for the subjects' arms, with the weakest illustrated in the left panel and the strongest in the right panel. The solid circles indicate the MVC along each of the measurement directions, while the open circles show the forces generated by triceps stimulation. The thick solid lines denote the orientations of the upper arm and forearm. Note that all results are referenced to a right arm configuration, even though arms C5$^-$ and C6 were on the left side. Data from the left arms have been mirrored about the vertical axis to facilitate comparisons across data sets.

For all subjects, the largest MVC was for forces directed toward the body. For the tested arm configuration, the elbow flexor muscles generated these forces. Elbow strength was similar across injury levels. Elbow flexion strength varied little

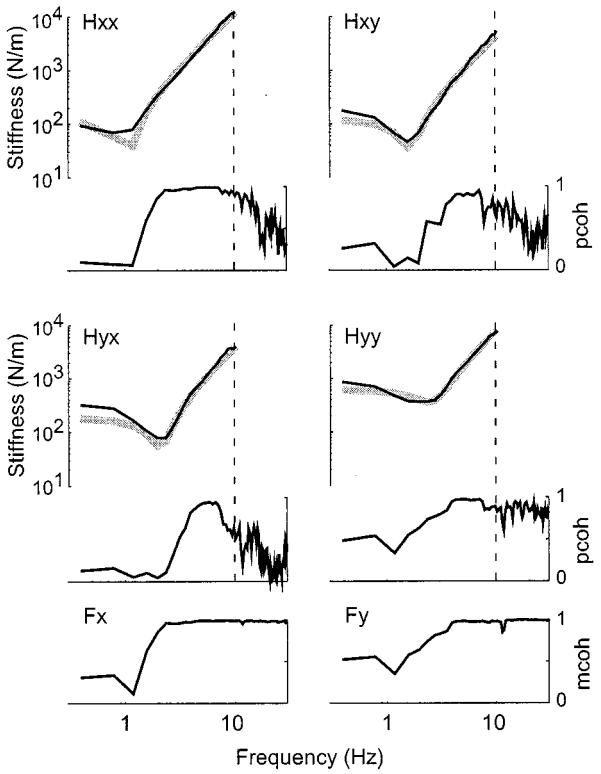

Fig. 6. Nonparametric transfer functions and coherence. The thin black lines illustrate typical estimated nonparametric stiffness transfer functions and the corresponding partial coherences relating endpoint displacements and endpoint forces. The bottom two figures are the multiple coherence functions for each output. Thick gray lines indicate the second-order parametric approximations to these transfer functions. Vertical dashed lined are drawn at 10 Hz, the highest frequency used in the parametric fit.

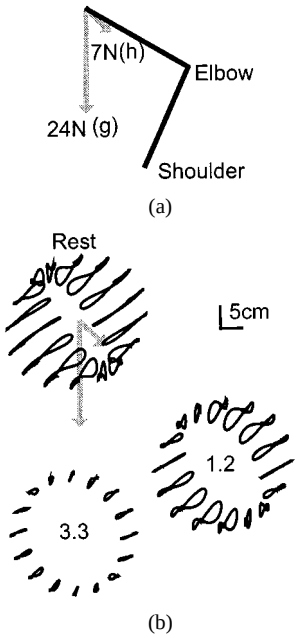

Fig. 7. C5$^-$ Dynamics during voluntary contraction. (a) Arm configuration and endpoint loads for which the endpoint stiffness dynamics were estimated; loads correspond to 20% of the MVC in each direction. (b) Three sets of endpoint trajectories simulated using arm parameters estimated from experimental data. Gray arrows are centered in the simulated trajectories for the rest dynamics and point to the simulated trajectories when the subject voluntarily exerted force in the indicated direction. Each trajectory represents the endpoint displacement for a $1N$ force impulse applied at the hand and oriented from the center of the trajectory toward the center of the ring of all trajectories. Numbers in the center of these two rings indicate the ratio of the average path length while the subject was at rest to that during the voluntary contractions.

and there was no voluntary elbow extension due to paralyzed extensor muscles in all subjects. The most significant impairment-related differences in voluntary endpoint force capability were due to shoulder function. Horizontal flexion (forces directed along the forearm toward the hand) was nonexistent in the weakest subject and small in the other two subjects. Horizontal shoulder extension (forces directed proximally along the forearm toward the elbow were small for the two C5 arms but increased substantially for the C6 arm. Overall, the range of directions over which significant voluntary forces could be generated increased progressively from the weakest to the strongest subjects. The areas of the shaded regions (which delimited the MVCs) for the two C5 subjects in Fig. 5 were 26% and 65% (C5$^-$ and C5$^+$, respectively) of the C6 subject.

B. Characterization of Endpoint Dynamics

The thin black lines in Fig. 6 illustrate the magnitude portions of typical nonparametric endpoint stiffness transfer functions. The linear nonparametric models of endpoint stiffness described the experimental data well, with an average multiple correlation coefficient (R^2) across all trials and all subjects of $91.6 \pm 5.8\%$. Fig. 6 also shows the second-order approximations to these functions (gray lines) and the corresponding partial (pcoh) and multiple coherences (mcoh). The multiple coherence functions remained high between 2.5 and 30 Hz, indicating that, over this frequency range, the endpoint force response to the applied position disturbances was accurately characterized by the nonparametric linear model. The partial coherences between each input and each output are shown below the corresponding transfer functions. For all subjects, partial coherence began to decline above approximately 10 Hz because almost no input power was applied beyond this limit [see Fig. 3(b)]. For this reason, parametric fits to the nonparametric transfer functions were performed only below 10 Hz, as indicated by the dashed lines in Fig. 6.

The overlap of the nonparametric transfer functions (thin black lines) and the associated second-order fits (thick gray lines) illustrated in Fig. 6 indicates that the endpoint dynamics estimated for this trial are well approximated by a system with inertial, viscous, and elastic components. The average parameter standard deviations for the inertial, viscous and elastic estimates were 0.040 N $\cdot$ s^2/m, 1.51 N $\cdot$ s/m and 34.6 N/m, respectively across all subjects and all endpoint loads. Inertia, viscosity and elasticity had magnitudes ranging up to 3 N $\cdot$ s^2/m, 40 N $\cdot$ s/m, and 1100 N/m, respectively.

C. Endpoint Dynamics During Voluntary Muscle Activation

Figs. 7–9 summarize the endpoint dynamics estimated during voluntary force exertion for each of the three arms. Fig. 7 summarizes these results for the weakest arm (C5$^-$). Fig. 7(a) shows the arm configuration during these tests as well as the load directions and load magnitudes for which endpoint stiffness dynamics were estimated. These loads correspond to 20% of the MVC in each direction; this arm was able to generate mea-

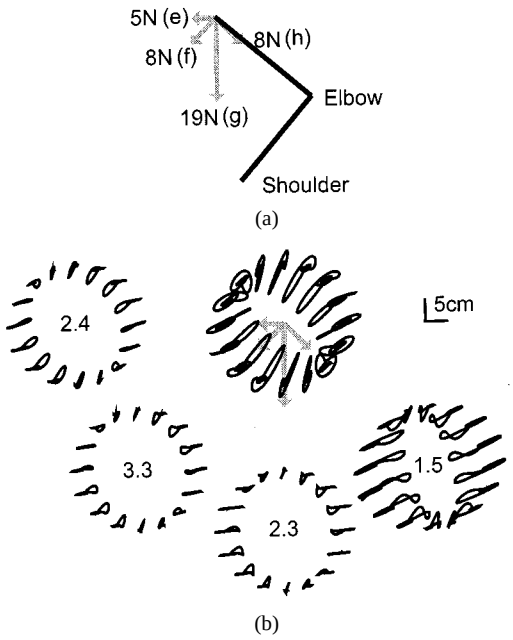

Fig. 8. $C5^{+}$ Dynamics during voluntary contraction. Format same as in Fig. 7.

surable voluntary forces in only two of the tested directions. Fig. 7(b) shows three sets of simulated endpoint trajectories, each forming in a ring. The gray arrows centered within the simulated hand trajectories for the passive (rest) case are repeated from Fig. 7(a). Each arrow points to the set of simulated hand trajectories generated for this voluntary force. The 16 endpoint trajectories in each set show the endpoint displacement for a $1N$ force impulse applied at the hand and oriented from the center of the trajectory toward the center of the ring. The numbers in the center of the two bottom rings indicate the ratio of the average path length while the subject was at rest to that during the voluntary contractions. Ratios greater than 1.0 correspond to a decreased average path length, i.e., increased endpoint stability relative to the rest case. For all conditions, the dominant endpoint motion was along the same axis. Elbow rotations resulted in endpoint trajectories orthogonal to the forearm axis and shoulder rotations resulted in trajectories orthogonal to the humeral axis. The dominant endpoint motion in Fig. 7(b) is orthogonal to neither of these axes and, hence, is due to rotations of both the elbow and shoulder joints. Perturbations applied to the hand while the arm was at rest resulted in large endpoint oscillations. The size of these oscillations decreased with voluntary force exertion, indicating an increase in arm stability, as shown by the path length ratios greater than 1.0.

Fig. 8 represents the endpoint dynamics during voluntary force exertion for the $C5^{+}$ arm and has the same layout as Fig. 7. Note that this subject could generate forces in four of the eight tested directions. For this subject, the dominant orientation of the simulated endpoint trajectories depended upon the endpoint load. When the arm was at rest, the endpoint trajectory was almost orthogonal to the forearm, indicating that the motion was due primarily to elbow joint rotations. During voluntary contractions, however, the motion was not orthogonal to either the forearm or humerus, indicating that both elbow and shoulder rotations contributed to the simulated endpoint motion. Again, it is seen that endpoint stability increased with increases in voluntary exertion, although the direction of the endpoint load had a large effect on the degree of stability. The most stable response was obtained when the subject was exerting an endpoint force in direction (f), where the average path length was 3.3 times shorter than when the arm was at rest. Stability decreased as the endpoint load orientation rotated from this most stable direction toward the ends of the available range of directions. Note that the direction of maximum endpoint stability (f) did not correspond to the direction where the subject could generate the maximum endpoint force (g), indicating dissociation between force and stability under some conditions.

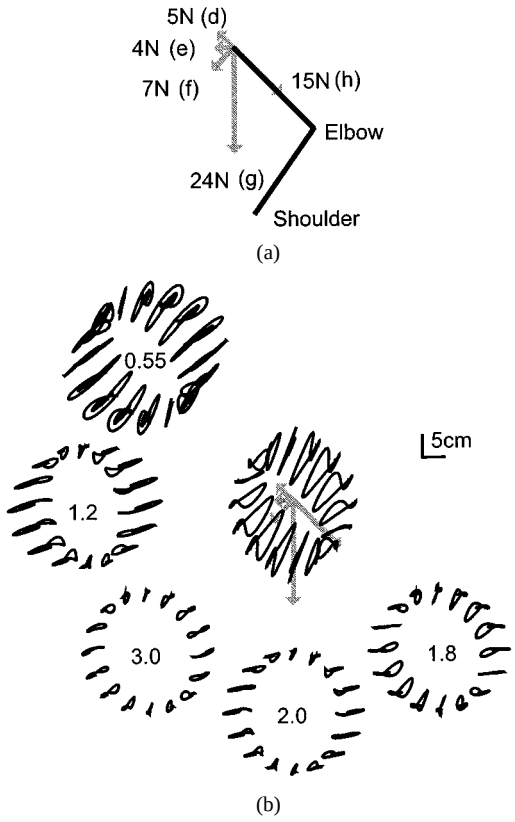

Fig. 9. C6 dynamics during voluntary contraction. Format same as in Fig. 7.

Fig. 9 represents the endpoint dynamics during voluntary force exertion for the strongest arm, C6, which had the greatest range of voluntary force generation. For this arm, the trajectory generated in response to the force impulses was dominated by elbow motion (movement orthogonal to forearm) when the arm was at rest and when the subject was pushing in direction (d). For all other directions, elbow motion was also accompanied by significant shoulder motion, as can be seen by the trajectory orientations that are orthogonal to neither the forearm nor the humerus. The voluntary force direction producing the greatest stability was (f). Again, stability decreased as the endpoint load orientation rotated from this most stable direction toward the ends of the available range of directions. Voluntary force generation increased endpoint stability relative to the rest case, except for when the subject was pushing along the axis of the forearm (d). In this case, endpoint stability decreased relative to the rest condition. As with the $C5^{+}$ arm, these results show that the force direction of maximum stability (f) differed from that of maximum strength (g).

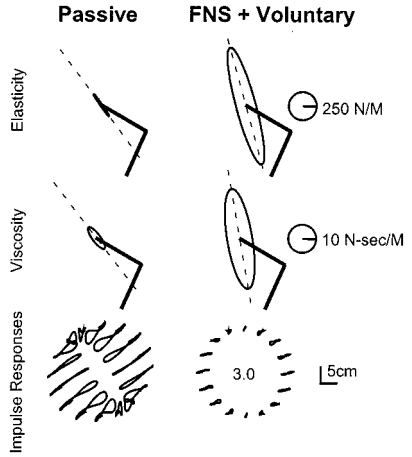

Fig. 10. Effects of triceps FNS with zero net force at endpoint. Shows typical results for a single arm C5$^-$ when the net force at the hand was zero. Results on the left are for when the arm was at rest and those on the right are for when the triceps was being stimulated and subjects voluntarily contracted flexor muscles to compensate for the FNS-induced extension moments, thereby generating no net endpoint force. The estimated endpoint elasticity, endpoint viscosity and arm configuration are shown at the top of the figure. The 2-D compliance impulse responses are shown at the bottom. The number in the FNS + voluntary trajectory ring is the ratio of average path length without stimulation to that with stimulation.

D. Endpoint Dynamics During Triceps FNS

Fig. 10 illustrates the effects of triceps FNS on endpoint stiffness and endpoint dynamics for a single arm, C5$^-$, when the net force at the hand was zero. For the results illustrated in the left passive column), the subject was at rest. The results in the right column (FNS + voluntary) were obtained while the subject voluntarily contracted the elbow and shoulder flexors to balance the moments ($\sim$ 10 Nm elbow extension and $\sim$ 5 Nm shoulder extension for this subject) produced by FNS of the triceps. Both conditions resulted in zero net endpoint force. The estimated endpoint elasticity and viscosity for these trials are shown by the ellipses in the top two rows of each column. Triceps FNS increased the magnitude of endpoint stiffness and endpoint viscosity and rotated the orientation of these ellipses clockwise, as is known to occur with increased elbow activation [15], [16]. The corresponding effects on the dynamic response to endpoint perturbations are summarized by the simulated trajectories shown at the bottom of the figure, which are similar to those presented in Figs. 7–9. The number in the FNS + voluntary trajectory ring is the ratio of the average trajectory path length with no stimulation to that during stimulation. The average path length decreased during triceps FNS by a factor of 3.0 for this arm and overall by an average of 2.3 across all arms. Thus, our results indicate that for a typical functional condition where triceps FNS is exactly balanced by voluntary co-contraction of the elbow flexors, both endpoint stiffness (ellipse size) and endpoint stability (decreased path length) are increased. Similar results were obtained when subjects exerted voluntary endpoint forces at 20% MVC in their strongest direction [direction (g) for all]. Again, the addition of triceps stimulation increased endpoint elasticity and viscosity and rotated the direction of maximum elasticity and viscosity clockwise. Under these conditions, the average path length decrease for all arms was 1.4.

IV. Discussion

This work investigated human arm stability following cervical SCI and how this stability can be modified by triceps FNS. Motor impairments of the upper limb due to SCI significantly limit the workspace where individuals can maintain stable hand positions and, hence, restrict their ability to perform normal activities of daily living. FNS is a means by which some of this lost function can be restored. Most of the rehabilitative efforts to use FNS following cervical SCI have focused on the hand [21], [28], but more recent studies have demonstrated that FNS can restore proximal arm functions [9], [10]. Restoration of proximal arm control requires both adequate strength to complete the desired task and sufficient stability to counter unanticipated external disturbances. Although arm strength can be measured easily, arm stability is more difficult to quantify. This work presented a method for quantifying arm dynamics and used this method to examine postural arm stability following cervical SCI.

Endpoint stiffness estimates were used to quantify postural arm dynamics. Dynamic endpoint stiffness characterizes the mechanical interface that humans use to interact with their environment. It describes the relationship between externally applied displacements of the hand and the forces generated in response and is thus thought to provide a quantitative measure of postural stability [11]–[16]. Understanding how this mechanical interface is modified following cervical SCI and how it can be manipulated via FNS may provide valuable insight for the design of improved upper extremity neuroprostheses.

Our specific findings were that: 1) the endpoint dynamics of the SCI-impaired arm can be adequately described by a linear model with inertial, viscous and elastic parameters; 2) variations in endpoint force capability across subjects with a range of cervical SCI levels (from weak C5 to strong C6) were due primarily to differences in shoulder strength; 3) there were differences between the force directions where the arm was strongest and where it was most stable; and 4) triceps FNS improved arm stability for all tested conditions.

A. Impairment Related Differences in Endpoint Force Production

As expected, the endpoint force directions and magnitudes that could be generated depended on each subject's impairment level. The observed differences resulted primarily from differences in shoulder horizontal flexion-extension strength, which increased progressively with decreasing impairment. None of the tested arms had voluntary elbow extension and voluntary elbow flexion strength was similar across the tested subjects. These results indicate that the force generating capabilities of the weakest arms could be most improved by increasing shoulder strength along with elbow extension strength. Combining FNS of the shoulder musculature with the existing triceps neuroprosthesis would provide one means of restoring this function.

B. Quantification of Dynamic Endpoint Stiffness

To better understand the control of arm mechanics following cervical SCI, we examined dynamic endpoint stiffness while each subject exerted constant, voluntary endpoint forces against the manipulator. We used stochastic perturbations to

facilitate efficient estimation of the stiffness dynamics. Similar techniques have been used to study able-bodied arm control [13]–[16], but have only recently been applied to the study of arm stability following cervical SCI [29]. We found that the endpoint dynamics of the arm following SCI were linear and well described by a parametric model with inertial, viscous, and elastic components, as previously reported for the able-bodied arm.

C. Endpoint Stability During Voluntary Muscle Activation

In most cases, increased voluntary effort led to increased endpoint stability, as measured by the decreased path length during simulated postural perturbations. The degree of stability, though, was dependent upon the orientation of the voluntarily generated endpoint force. The stiffness and viscosity of individual muscles [30], [31], single joints [32], and multijoint systems [15], [33] are known to increase with increases in muscle force, but the damping associated with these changes remains nearly constant under isometric conditions [33]–[35]. Hence, we expected our measure of stability (path length) to be closely related to the total force applied at the hand. To the contrary, our results demonstrated a clear dissociation between the direction of maximum stiffness and that of maximum strength. Two of the three tested arms were most stable when exerting forces in a direction other than where they were strongest. The third arm, C5^{-}, could not generate force in the direction where the two stronger arms were most stable due to limited shoulder strength. Hence, these results indicate that the shoulder musculature plays an important role not only for generating endpoint forces, but also for maintaining stable endpoint postures.

It is likely that two primary mechanisms produced the observed relationship between endpoint force orientation and postural stability. First, the subjects in this study have scattered paralysis and weakness of the shoulder and elbow musculature and, thus probably do not have the redundancy needed to co-contract muscles at these joints to generate the specified endpoint forces while simultaneously producing desirable stability properties. Thus, endpoint stiffness (and, hence, stability) will be determined in the SCI subjects almost exclusively by the endpoint force direction. The observed decrease in stability observed for force directions where voluntary capacity was quite low supports this hypothesis. Second, the subjects examined here lacked voluntary elbow extension and, thus, were able to voluntarily adjust only the elbow flexion moment. External loads directed toward the shoulder and elbow joints are known to decrease arm stability, whereas those directed away from these joints increase arm stability, through a pendulum-like phenomenon [36]. This phenomenon may explain why we observed decreases in arm stability relative to passive conditions when the C6 arm exerted forces along the axis of the forearm (see Fig. 9).

D. FNS-Induced Changes in Endpoint Stability

The effects of triceps FNS on endpoint stability were investigated by comparing the changes in stability that occurred due to FNS under two experimental conditions, with no net endpoint force at the hand and with subjects pulling at 20% MVC in the direction that they were strongest. Triceps FNS increased stability during both tasks. The most significant increases in stability due to triceps FNS occurred for the no-load condition, because there was little voluntary muscle activity in the absence of triceps FNS. This increased stability was due to the increased elasticity and viscosity associated with the increased muscle activity. By providing a functional level of triceps extension moment [4], [9], [10], the triceps neuroprosthesis increases the directions in which endpoint forces can be generated *and* increases endpoint stability throughout this range.

E. Functional Relevance of Endpoint Stiffness

Arm control during functional activities requires the ability to maintain stable arm postures, to move between these postures and to interact with a variety of external objects and forces. To achieve these goals, individuals must have sufficient strength, stability and coordination. We have begun to address these issues by examining the effects of strength and stability on the ability to maintain stable postures. Our results indicate that both are likely to be critical to future efforts to improve function through the use of FNS. In particular, the additional information provided by the stiffness estimates obtained here should provide invaluable information in the development of task-specific FNS control mechanisms that provide high stiffness when desirable and low stiffness when that is more appropriate. Although these results are encouraging, we have not yet examined the relationship between functional performance and endpoint stiffness. Therefore, the full impact of this work will not be realized until these effects have been addressed by investigating functional tasks that require not only the maintenance of stable postures, but also coordinated movement between these postures.

ACKNOWLEDGMENT

The authors would like to thank A. Bryden and B. Memberg for their assistance and valuable comments during this project.

REFERENCES

[1] J. Bateman and V. Fornasier, *The Shoulder and Neck*. Philadelphia, PA: Saunders, 1978.

[2] R. D. Welch, S. J. Lobley, S. B. O'Sullivan, and M. M. Freed, "Functional independence in quadriplegia: Critical levels," *Arch. Phys. Med. Rehabil.*, vol. 67, pp. 235–240, 1986.

[3] D. A. Demagone, R. D. Zafonte, G. Herbison, and J. Ditunno, "Triceps strength as a predictor of daily self-care in quadriplegics (abstract)," *J. Amer. Paraplegia Soc.*, vol. 14, pp. 95–96, 1991.

[4] A. M. Bryden, W. D. Memberg, and P. E. Crago, "Electrically stimulated elbow extension in persons with C5/C6 tetraplegia: A functional and physiological evaluation [In Process Citation]," *Arch. Phys. Med. Rehabil.*, vol. 81, pp. 80–88, 2000.

[5] C. A. Wijman, K. C. Stroh, C. L. Van Doren, G. B. Thrope, P. H. Peckham, and M. W. Keith, "Functional evaluation of quadriplegic patients using a hand neuroprosthesis," *Arch. Phys. Med. Rehabil.*, vol. 71, pp. 1053–1057, 1990.

[6] M. J. Mulcahey, R. R. Betz, B. T. Smith, A. A. Weiss, and S. E. Davis, "Implanted functional electrical stimulation hand system in adolescents with spinal injuries: An evaluation," *Arch. Phys. Med. Rehabil.*, vol. 78, pp. 597–607, 1997.

[7] D. Popovic, A. Stojanovic, A. Pjanovic, S. Radosavljevic, M. Popovic, S. Jovic, and D. Vulovic, "Clinical evaluation of the Bionic Glove," *Arch. Phys. Med. Rehabil.*, vol. 80, pp. 299–304, 1999.

[8] N. Hoshimiya, A. Naito, M. Yajima, and Y. Handa, "A multichannel FES system for the restoration of motor functions in high spinal cord injury patients: A respiraition-controlled system for multijoint upper extremity," *IEEE Trans. Biomed. Eng.*, vol. 36, pp. 754–760, July 1989.

[9] P. E. Crago, W. D. Memberg, M. K. Usey, M. W. Keith, R. F. Kirsch, G. J. Chapman, M. A. Katorgi, and E. J. Perreault, "An elbow extension neuroprosthesis for individuals with tetraplegia," *IEEE Trans. Rehabil. Eng.*, vol. 6, pp. 1–6, Mar. 1998.
[10] J. H. Grill and P. H. Peckham, "Functional neuromuscular stimulation for combined control of elbow extension and hand grasp in C5 and C6 quadriplegics," *IEEE Trans. Rehabil. Eng.*, vol. 6, pp. 190–199, June 1998.
[11] N. Hogan, "The mechanics of multi-joint posture and movement control," *Biol. Cybern.*, vol. 52, pp. 315–331, 1985.
[12] F. Lacquaniti, M. Carrozzo, and N. A. Borghese, "Time-varying mechanical behavior of multijointed arm in man," *J. Neurophysiol.*, vol. 69, pp. 1443–1463, 1993.
[13] J. M. Dolan, M. B. Friedman, and M. L. Nagurka, "Dynamic and loaded impedance components in the maintenance of human arm posture," *IEEE Trans. Syst., Man, Cybern.*, vol. 23, pp. 698–709, May/June 1993.
[14] T. Tsuji, P. G. Morasso, K. Goto, and K. Ito, "Hand impedance characteristics during maintained posture," *Biol. Cybern.*, vol. 72, pp. 475–485, 1995.
[15] H. Gomi and R. Osu, "Task-dependent viscoelasticity of human multijoint arm and its spatial characteristics for interaction with environments," *J. Neurosci.*, vol. 18, pp. 8965–8978, 1998.
[16] E. J. Perreault, R. F. Kirsch, and P. E. Crago, "Effects of voluntary force generation on the elastic components of endpoint stiffness," *Exp. Brain Res.*, vol. 141, pp. 312–323, 2001.
[17] E. J. Perreault, R. F. Kirsch, and A. M. Acosta, "Multiple-input, multiple-output system identification for the characterization of limb stiffness dynamics," *Biol. Cybern.*, vol. 80, pp. 327–337, 1999.
[18] *Standards for Neurological and Functional Classification of Spinal Cord Injury*, American Spinal Injury Association, International Medical Society of Paraplegia, Atlanta, GA, 1992.
[19] C. L. McDowell, E. A. Moberg, and J. H. House, "The second international conference on surgical rehabilitation of the upper limb in tetraplegia (quadriplegia)," *J. Hand Surg.*, vol. 11A, p. 604, 1986.
[20] K. S. Wuolle, C. L. Van Doren, G. B. Thrope, M. W. Keith, and P. H. Peckham, "Development of a quantitative hand grasp and release test for patients with tetraplegia using a hand neuroprosthesis," *J. Hand Surg. [Amer.]*, vol. 19, pp. 209–218, 1994.
[21] M. W. Keith, P. H. Peckham, G. B. Thrope, K. C. Stroh, B. Smith, J. R. Buckett, K. L. Kilgore, and J. W. Jatich, "Implantable functional neuromuscular stimulation in the tetraplegic hand," *J. Hand Surg.*, vol. 14A, pp. 524–530, 1989.
[22] P. Peckham, J. T. Mortimer, and E. B. Marsolais, "Alteration in the force and fatigability of skeletal muscle in quadriplegic humans following exercise induced by chronic electrical stimulation," *Clin. Orthopaed. Rel. Res.*, vol. 114, pp. 326–334, 1976.
[23] A. M. Acosta, R. F. Kirsch, and E. J. Perreault, "A robotic manipulator for the characterization of two-dimensional dynamic stiffness using stochastic displacement perturbations," *J Neurosci. Methods*, vol. 102, pp. 177–186, 2000.
[24] K. A. Mann, F. W. Werner, and A. K. Palmer, "Frequency spectrum analysis of wrist motion for activities of daily living," *J. Orthoped. Res.*, vol. 7, pp. 304–306, 1989.
[25] S. Stroeve, "Impedance characteristics of a neuromusculoskeletal model of the human arm I. Posture control," *Biol. Cybern.*, vol. 81, pp. 475–494, 1999.
[26] P. Z. Marmarelis and V. Z. Marmarelis, *Analysis of Physiological Systems*. New York: Plenum, 1978.
[27] F. A. Mussa-Ivaldi, N. Hogan, and E. Bizzi, "Neural, mechanical and geometric factors subserving arm posture in humans," *J. Neurosci.*, vol. 5, pp. 2732–2743, 1985.
[28] P. E. Crago, R. J. Nakai, and H. J. Chizeck, "Feedback regulation of hand grasp opening and contact force during stimulation of paralyzed muscle," *IEEE Trans. Biomed. Eng.*, vol. 38, pp. 17–28, Jan. 1991.
[29] E. J. Perreault, A. M. Acosta, R. F. Kirsch, and P. E. Crago, "Using estimates of dynamic endpoint stiffness to quantify the effects of triceps functional neuromuscular stimulation," in *Proc. Int. Functional Electrical Stimulation Society Conf.*, Vancouver, BC, Canada, 1997, pp. 137–138.
[30] J. A. Hoffer and S. Andreassen, "Regulation of soleus muscle stiffness in premammillary cats: Intrinsic and reflex components," *J. Neurophysiol.*, vol. 45, pp. 267–285, 1981.
[31] R. F. Kirsch, D. Boskov, and W. Z. Rymer, "Muscle stiffness during transient and continuous movements of cat muscle: Perturbation characteristics and physiological relevance," *IEEE Trans. Biomed. Eng.*, vol. 41, pp. 758–770, Aug. 1994.
[32] R. E. Kearney and I. W. Hunter, "System identification of human joint dynamics," *CRC Crit. Rev. Biomed. Eng.*, vol. 18, pp. 55–87, 1990.
[33] Ph.D. dissertation, Case Western Reserve Univ., Cleveland, OH, 2000.
[34] G. C. Agarwal and G. L. Gottlieb, "Compliance of the human ankle joint," *J. Biomech. Eng.*, vol. 99, pp. 166–170, 1977.
[35] P. L. Weiss, I. W. Hunter, and R. E. Kearney, "Human ankle joint stiffness over the full range of muscle activation levels," *J. Biomech.*, vol. 21, pp. 539–544, 1988.
[36] J. McIntyre, F. A. Mussa-Ivaldi, and E. Bizzi, "The control of stable arm postures in the multi-joint arm," *Exp. Brain Res.*, vol. 110, pp. 248–264, 1996.

Eric J. Perreault (S'97–M'00) received the B.Eng. and M.Eng. degrees in electrical engineering from McGill University, Montréal, QC, Canada, in 1989 and 1992, respectively, and the Ph.D. in biomedical engineering from Case Western Reserve University, Cleveland, OH, in 2000.

From 1993 to 1995, he worked in industry as a Control Systems and Design Engineer. Currently, he is a Postdoctoral Fellow in the Department of Physiology at Northwestern University, Evanston, IL. His research focuses on the neural control of multijoint movement, task-dependent strategies for neural control, muscle mechanics, and system identification of physiological systems.

Patrick E. Crago (S'66–M'67) received the B.S. degree in electrical engineering from Carnegie-Mellon University, Pittsburgh, PA, in 1967 and the M.S. and Ph.D. degrees in biomedical engineering from Case Western Reserve University (CWRU), Cleveland, OH, in 1970 and 1973, respectively.

He did Postdoctoral studies in neuromuscular physiology in the Department of Physiology at Johns Hopkins University, Baltimore, MD. In 1976, following his Postdoctoral studies, he returned to CWRU as a Senior Research Associate, and in 1982, he joined the Biomedical Engineering faculty as an Assistant Professor. He was promoted to Associate Professor and Professor in 1987 and 1992, respectively. He is currently the Allen H. and Constance T. Ford Professor of Biomedical Engineering and Chairman of the department. His research interests are in restoration of movement by functional neuromuscular stimulation and in normal and pathological movement control and regulation. Current research projects include biomechanical, neural and neuroprosthetic control of the wrist, forearm, and elbow, and the clinical implementation and evaluation of neuroprostheses for hand grasp and proximal arm control. His research is funded by the National Institutes of Health and the Department of Veterans Affairs. His research laboratory is located in the Rehabilitation Engineering Center at MetroHealth Medical Center, which is part of the Cleveland FES Center.

Dr. Crago is a member of the IEEE Engineering in Medicine and Biology Society, the American Society for Biomechanics, the Society for Neuroscience, the American Association for the Advancement of Science, and the International FES Society.

Robert F. Kirsch (S'80–M'82) received the B.S. degree from the University of Cincinnati, Cincinatti, OH, in 1982 and the M.S. and Ph.D. degrees from Northwestern University, Evanston, IL, in 1986 and 1990, respectively.

He completed a Postdoctoral Fellowship at McGill University, Montréal, QC, Canada, in 1993. He is currently an Assistant Professor in the Department of Biomedical Engineering at Case Western Reserve University, Cleveland, OH, and a Biomedical Engineer at the Cleveland Veterans Affairs Medical Center. His research focuses on the neural control of movement, restoring movement through the use of functional neuromuscular stimulation and musculoskeletal modeling of the human body.